



---

**Willmott AJ, Pascual-Ahuir EG.**

**[Planetary and gravity waves in a polar basin.](#)**

***Journal of Physical Oceanography* 2017, 47(6), 1433-1440.**

**Copyright:**

© [Copyright 2017 AMS.](#)

**DOI link to article:**

<https://doi.org/10.1175/JPO-D-16-0253.1>

**Date deposited:**

24/03/2017

**Embargo release date:**

08 December 2017

# Planetary and gravity waves in a polar basin

Andrew J. Willmott\* and Estanislao Gavilan Pascual-Ahuir

*Newcastle University, Newcastle upon Tyne, United Kingdom*

Revised February, 2017

\**Corresponding author address:* Andrew J. Willmott, School of Marine Science and Technology,

Newcastle University, Newcastle upon Tyne, NE1 7RU.

E-mail: [andrew.willmott@newcastle.ac.uk](mailto:andrew.willmott@newcastle.ac.uk)

## ABSTRACT

8    The eigenfrequencies of freely propagating barotropic, divergent, planetary  
9    waves and gravity waves in a spherical polar cap are presented using an ap-  
10    proximation in which full spherical geometry is retained in the derivation of  
11    the wave amplitude equation. Subsequently, the co-latitude angle in the coef-  
12    ficients of the wave amplitude equation is fixed, thereby allowing the eigen-  
13    value problem to be solved using analytical methods. The planetary wave  
14    frequencies are compared with published results that adopt the polar-plane  
15    approximation to solve the equivalent free-wave problem. Low order plane-  
16    tary waves frequencies calculated in this study agree well with the polar-plane  
17    approximation results. The sensitivity of the wave frequencies to the choice  
18    of the fixed co-latitude in the coefficients of the wave amplitude equation is  
19    discussed.

## 20 1. Introduction

21 The analytical treatment of atmospheric or oceanic dynamics in a polar basin centered at the pole  
22 is hindered by the non-uniform meridional gradient of the Coriolis parameter. LeBlond (1964)  
23 illustrate this point in developing the “polar plane approximation”. The Coriolis parameter,  $f =$   
24  $2\Omega \cos \theta$ , where  $\Omega$  is the angular velocity of the rotation of the Earth and  $\theta$  is the co-latitude. In  
25 terms of plane polar coordinates  $r, \varphi$  in the plane of projection, tangent to the Earth at the pole, we  
26 observe that

$$\begin{aligned} f &= 2\Omega \left( 1 - \frac{\theta^2}{2} + \dots \right), \\ &= 2\Omega \left( 1 - \frac{1}{2} \left( \frac{r}{R} \right)^2 + \dots \right), \end{aligned} \quad (1.1)$$

27 where  $R$  is the radius of the Earth. For dynamics on the “polar plane” with horizontal length scales  
28 satisfying the constraint

$$\left( \frac{r}{R} \right)^2 \ll 1,$$

29 LeBlond (1964) introduces the approximation

$$f \approx 2\Omega,$$

$$\frac{df}{dr} \approx -\frac{2\Omega r}{R^2},$$

31 which follows immediately from (1.1). Therefore, starting with one of the simplest analogues  
32 for a polar ocean on a polar plane, namely a homogeneous fluid, we predict that the barotropic  
33 potential vorticity equation will have non-constant coefficients. Nevertheless, LeBlond (1964)  
34 obtains the dispersion relation for divergent barotropic planetary waves in a flat bottom polar  
35 basin. In related meteorological studies, Haurwitz (1975) and Bridger and Stevens (1980) use  
36 cylindrical polar coordinates to study freely propagating waves in a high-latitude atmosphere. The  
37 concept of the delta ( $\delta$ )-plane approximation for quasi-geostrophic dynamics at high latitudes was

38 developed by Harlander (2005). Harlander (2005) demonstrates that the high-latitude  $\delta$ -plane  
39 model can be consistently derived from spherical geometry. On the  $\delta$ -plane Harlander (2005)  
40 demonstrates that high-latitude Rossby waves energy rays are curved, which is not the case on the  
41  $\beta$ -plane.

42  
43 In contrast with studies of free-waves in a polar basin there is a considerable body of liter-  
44 ature on free-waves in a thin layer of fluid on the entire rotating earth. For example, Paldor et al.  
45 (2013) and Paldor (2015) obtain solutions for zonally propagating planetary and inertial-gravity  
46 (i.e. Poincaré) waves on the entire rotating earth, extending the solutions in the seminal work of  
47 Longuet-Higgins (1968).

48  
49 In this paper we present a new method for obtaining the dispersion relation for freely prop-  
50 agating barotropic gravity and planetary waves in a polar basin. The computationally efficient  
51 dispersion relation is derived using a somewhat overlooked approximation, first proposed by  
52 Imawaki and Takano (1974), in their analysis of source-sink driven planetary geostrophic dynam-  
53 ics in a polar basin. Gavilan Pascual-Ahuir (2017, personal communication) uses the Imawaki  
54 and Takano (1974) approximation to analytically derive solutions for planetary geostrophic  
55 steady circulation driven by prescribed inflow/outflow at the boundary of a circular basin with  
56 simple shelf topography. We will hereafter adopt the phrase “IT approximation” in which the  
57 linearised spherical shallow water equations are used to derive the barotropic vorticity equation,  
58 and thereafter the co-latitude is fixed in the coefficients of this partial differential equation; an  
59 approach first discussed by Imawaki and Takano (1974), as far as the authors are aware. How  
60 well does the IT approximation capture the dynamics of freely propagating gravity and divergent  
61 planetary waves in a polar basin? This question is addressed in this paper which is structured

as follows. Section 2 derives the eigenvalue problem for gravity and planetary waves using the IT approximation. Subsequently, planetary waves are discussed in Section 3, gravity waves are discussed in Section 4, followed by conclusions in Section 5.

## 2. Formulation of the eigenvalue problem

We consider an ocean of uniform density on a polar cap with centre located at the pole. A spherical polar coordinates system is adopted where  $\theta$  and  $\varphi$  denote the co-latitude and longitude angles, respectively. Let  $\theta_B$  denote the co-latitude of the boundary of the polar basin. Then,  $\theta \in [0, \theta_B)$  and  $\varphi \in [0, 2\pi)$ . The unit vectors  $\{\mathbf{k}, \hat{\boldsymbol{\theta}}, \hat{\boldsymbol{\varphi}}\}$  form a right-handed triad, where

$$\mathbf{k} \wedge \hat{\boldsymbol{\theta}} = \hat{\boldsymbol{\varphi}},$$

and  $\mathbf{k}$  is a unit vector in the (outward) radial direction (see Figure 1). With respect to this coordinates system the linearised shallow water equations for inviscid homogeneous dynamics in the polar cap take the form

$$u_t + fv = -\frac{g}{R \sin \theta} \eta_\varphi, \quad (2.1a)$$

$$v_t - fu = -\frac{g}{R} \eta_\theta, \quad (2.1b)$$

$$\eta_t + \frac{1}{R \sin \theta} \left[ (Hu)_\varphi + (Hv \sin \theta)_\theta \right] = 0, \quad (2.1c)$$

where the velocity  $\mathbf{u} = u\hat{\boldsymbol{\varphi}} + v\hat{\boldsymbol{\theta}}$ ,  $\eta$  is the free surface elevation,  $H$  is the undisturbed depth of the ocean,  $g$  is the gravitational acceleration,  $f = 2\Omega \cos \theta$ , where  $\Omega$  is the angular frequency of the rotation of the Earth and  $R$  is the radius of the Earth. We seek azimuthally propagating waves

78 solutions of (2.1) of the form

$$\left. \begin{aligned} u &= U(\theta) \exp[i(m\varphi - \omega t)] \\ v &= V(\theta) \exp[i(m\varphi - \omega t)] \\ \eta &= F(\theta) \exp[i(m\varphi - \omega t)] \end{aligned} \right\} \quad (2.2)$$

79 where  $\omega > 0$  is the angular wave frequency,  $m$  is the azimuthal integer wave number (i.e  $m =$   
80  $\pm 1, \pm 2, \pm 3, \dots$ ) and  $U$ ,  $V$  and  $F$  are amplitude functions. Substituting (2.2) in (2.1) we obtain

$$-i\omega U + fV = -\frac{img}{R \sin \theta} F, \quad (2.3a)$$

$$-i\omega V - fU = -\frac{g}{R} F', \quad (2.3b)$$

$$-i\omega F + \frac{1}{R \sin \theta} [imHU + (HV \sin \theta)_\theta] = 0, \quad (2.3c)$$

82 where  $F' \equiv dF/d\theta$ . From (2.3a,b) we find that

$$U = \frac{g \left( fF' - \frac{m\omega}{\sin \theta} F \right)}{R\mathcal{D}}, \quad (2.4a)$$

$$V = \frac{ig \left( \omega F' - \frac{mf}{\sin \theta} F \right)}{R\mathcal{D}}, \quad (2.4b)$$

83 where  $\mathcal{D} \equiv f^2 - \omega^2$ . Upon substituting (2.4) into (2.3c), and after some lengthy algebra, we obtain  
84 the wave amplitude equation for freely-propagating waves in polar cap:

$$\begin{aligned} F'' + \left\{ \frac{\sin 2\theta}{\cos^2 \theta - \sigma^2} + \cot \theta \right\} F' - \left\{ \frac{m}{\sigma} \left( \frac{\cos^2 \theta + \sigma^2}{\cos^2 \theta - \sigma^2} \right) \right. \\ \left. + \frac{m^2}{\sin^2 \theta} + \left( \frac{R}{r_e} \right)^2 (\cos^2 \theta - \sigma^2) \right\} F = 0, \end{aligned} \quad (2.5a)$$

85 where

$$\sigma = \frac{\omega}{2\Omega}, \quad r_e^2 = \frac{gH}{4\Omega^2}. \quad (2.5b)$$

86 We note that  $\sigma$  is the dimensionless wave frequency and that  $r_e$  is the external Rossby radius of  
87 deformation. On the basin wall we demand that there is no normal flow:

$$V = 0 \quad \text{on} \quad \theta = \theta_B,$$

88 which can be expressed as

$$F' - \frac{m}{\sigma} \cot \theta F = 0, \quad \text{on } \theta = \theta_B, \quad (2.6)$$

89 upon using (2.4b). At the pole (2.5a) reduces to

$$F(0) = 0. \quad (2.7)$$

90 We now invoke the IT approximation and let  $\theta = \theta_0$ , where  $0 < \theta_0 < \theta_B$ , in the coefficients  
 91 of (2.5a) thereby obtaining a constant coefficient second order ordinary differential equation.  
 92 Typically, we let  $\theta_0 = 0.5\theta_B$ , but the sensitivity of the free-wave dispersion relations to this angle  
 93 will be discussed later. Equation (2.5a) together with boundary conditions (2.6) and (2.7) form a  
 94 Sturm-Liouville eigenvalue problem for  $\sigma$ .

95

96 Before analysing this eigenvalue problem in the subsequent sections, it is instructive to  
 97 consider how the amplitude equations (2.5a) is modified when variations of  $f$  with co-latitude are  
 98 suppressed. An approximation of this type in a spherical polar basin would be valid for small  
 99 wavelength waves in the meridional directions. When  $f = 2\Omega$ , the amplitude equation simplifies  
 100 to

$$F'' + \cot \theta F' - \left\{ \frac{m^2}{\sin^2 \theta} + \left( \frac{R}{r_e} \right)^2 (1 - \sigma^2) \right\} F = 0. \quad (2.8)$$

101 Comparing (2.8) with (2.5a) we observe that

$$\frac{\sin 2\theta}{\cos^2 \theta - \sigma^2} \quad ; \quad \frac{m}{\sigma} \left( \frac{\cos^2 \theta + \sigma^2}{\cos^2 \theta - \sigma^2} \right),$$

102 arise from the variation of the Coriolis parameter with co-latitude. On the “ $f$ -sphere”, we noted  
 103 that  $f = 2\Omega$  (retaining the first term in the Maclaurin expansion in powers of  $\theta$ ) which leads to the  
 104 modification of the term involving  $r_e$  in (2.5a).



### 105 3. Planetary waves ( $\sigma^2 \ll 1$ )

106 For these low frequency waves (2.5a) can be approximated as

$$F'' + AF' - BF = 0, \quad (3.1)$$

107 where

$$A \equiv 2 \tan \theta_0 + \cot \theta_0 > 0$$

108 and

$$B \equiv \frac{m}{\sigma} + \frac{m^2}{\sin \theta_0} + \left( \frac{R}{r_e} \right)^2 \cos^2 \theta_0$$

109 We observe that if the meridional structure of these wave modes is to be oscillatory then we require

110  $m < 0$ . The general solution of (3.1) will then take the form:

$$F = \exp \left( -\frac{1}{2} A \theta \right) [c_1 \cos(\kappa \theta) + c_2 \sin(\kappa \theta)], \quad (3.2)$$

111 where

$$\kappa^2 = -B - (1/4)A^2,$$

112 and  $c_1, c_2$  are arbitrary constants. Notice that since  $m < 0$ , (2.2) reveals that the phase velocity of  
 113 the waves is westward (i.e. in the negative  $\varphi$  sense) as expected for planetary waves. Application  
 114 of (2.6) and (2.7) to (3.2) yields the dispersion relation for divergent barotropic planetary waves in  
 115 spherical cap using the IT approximation:

$$\kappa = \left[ \frac{m}{\sigma} \cot \theta_B + \frac{1}{2} A \right] \tan(\kappa \theta_B), \quad (3.3)$$

116 For a given value of  $m (< 0)$  the discrete set of roots  $\sigma_{m,n} (n = 1, 2, 3, \dots)$  can be determined numer-  
 117 ically from (3.3). However, approximate values of the roots are readily obtained from (3.3) upon  
 118 noting that when  $\sigma \ll 1$  the dispersion relation can be approximated by

$$m \cot \theta_B \tan(\kappa \theta_B) = 0,$$

119 whence

$$\kappa_n \approx \frac{n\pi}{\theta_B}, \quad n = 1, 2, \dots \quad (3.4)$$

120 Using the expression for  $\kappa$ , (3.4) yields the approximate values for  $\sigma_{m,n}$ :

$$\frac{|m|}{\sigma_{m,n}} = \left( \frac{n\pi}{\theta_B} \right)^2 + \frac{m^2}{\sin^2 \theta_B} + \left( \frac{R}{r_e} \right)^2 \cos^2 \theta_0 + \sec^2 \theta_0 + (1/4) \cot^2 \theta_0. \quad (3.5)$$

121 Tables 2 presents the wave frequencies calculates from (3.3) using the ocean basin parameters  
 122 in LeBlond (1964) which are listed in Table 1. In this study we do not explicitly use the radius,  
 123  $r_B$ , of the basin as a parameter in contrast with the polar plane analysis of LeBlond (1964).  
 124 However,  $r_B = R \sin \theta_B$  and using the parameters in Table 1 we find that  $r_B = 1424$  km. We find  
 125 that the eigenfrequencies (3.5) are identical to those in Table 2 with the exception of  $\sigma_{-1,1}$  which  
 126 differs in the last decimal place. We observe from Table 3 that the low order planetary waves  
 127 modes are accurately represented using the IT approximation. More specially,  $\sigma_{-1,n}$  ( $n = 1, \dots, 5$ )  
 128 and  $\sigma_{-2,1}$  satisfying (3.3) are within 11% of the equivalent frequencies calculated by LeBlond  
 129 (1964). We also observe increasing discrepancies between the eigenfrequencies determined by  
 130 LeBlond (1964) and the IT approximation as the azimuthal and meridional wavelengths decrease,  
 131 corresponding to increasing  $|m|$  and  $n$ . This discrepancy reflects the fact that as the wavelengths  
 132 of the modes decrease, their structure becomes more sensitive to the choice of the co-latitude  $\theta_0$   
 133 in the dispersion relation. In practice, forced planetary waves generally have most of their energy  
 134 in the lowest modes for which (3.5) gives accurate predictions for the wave periods. The planetary  
 135 wave periods,  $T_{m,n} = \pi(\Omega\sigma_{m,n})^{-1}$ , and for the gravest mode,  $\sigma_{-1,1} = 153$  days using  $\sigma_{-1,1}$  in  
 136 Table 2. The structure of the eigenfunctions is qualitatively identical to those in LeBlond (1964)  
 137 and are therefore not reproduced here.

138

139 Figure 2 shows a plot of  $\sigma_{-1,n}$  ( $n = 1, \dots, 5$ ) as a function of  $\varepsilon^2 = (r_e/R)^2$ , when  $\theta_0 = 0.5\theta_B$ .

Varying  $\varepsilon$  is equivalent to varying the depth,  $H$ , of the ocean. The planetary wave frequencies in a polar basin are a monotonic functions of  $\varepsilon$ . Similar qualitative behaviour for the planetary wave eigenfrequencies on a sphere was noted by Longuet-Higgins (1968). Note that the asymptotic values of the eigenfrequencies  $\sigma_{-1,n}$ , in the limit of large  $H$ , are given by

$$\sigma_{-1,n} \rightarrow \left[ \left( \frac{n\pi}{\theta_B} \right)^2 + \frac{1}{\sin^2 \theta_B} + \sec^2 \theta_0 + (1/4) \cot^2 \theta_0 \right]^{-1}$$

How sensitive are the eigenfrequencies that are accurately approximated by the dispersion relation (3.3) to the value of  $\theta_0$ ? It is clear from (3.5) that for “large”  $|m|$  and  $n$  the sensitivity of the eigenfrequencies to the values of these modal numbers will be small. To quantify this assertion Table 4 shows  $|\sigma_{m,n}(0.75\theta_B) - \sigma_{m,n}(0.5\theta_B)| / \sigma_{m,n}(0.5\theta_B)$ , expressed as a percentage. Entries below the principal diagonal in Table 4 show decreasing sensitivity of the eigenvalues to the value of  $\theta_0$ . In practice, we are interested in the sensitivity of  $\sigma_{-1,n}$  ( $n = 1, \dots, 5$ ) and  $\sigma_{-2,1}$  to  $\theta_0$ , because they are a good approximation to the exact values. Clearly, the gravest mode eigenfrequency given by (3.5) provides an accurate approximation to the exact value when  $\theta_0 = 0.5\theta_B$ . Other values of  $\theta_0 \in (0, \theta_B]$  reduce the accuracy of this frequency. On the other hand,  $\sigma_{-1,4}$  and  $\sigma_{-1,5}$  are relatively insensitive to  $\theta_0$  and provide acceptable approximations to their exact values. A final remark about the choice of  $\theta_0$  is that an alternative measure of frequency sensitivity to this angle is  $|\sigma_{m,n}(0.25\theta_B) - \sigma_{m,n}(0.5\theta_B)| / \sigma_{m,n}(0.5\theta_B)$ . However, (3.5) shows that as  $\theta_0 \rightarrow 0$  the dispersion relation will become singular. The simple message is to therefore, “stay away from the pole”, using the IT approximation.

#### 4. Gravity waves ( $\sigma > 1$ )

For the high frequency gravity modes we re-write the amplitude equation (2.5a) as

$$F'' + PF' + QF = 0, \tag{4.1}$$

160 where

$$P \equiv \frac{\sin 2\theta_0}{\cos^2 \theta_0 - \sigma^2} + \cot \theta_0,$$

161 and

$$Q \equiv \left(\frac{R}{r_e}\right)^2 (\sigma^2 - \cos^2 \theta_0) - \frac{m^2}{\sin^2 \theta_0} - \frac{m}{\sigma} \left(\frac{\cos^2 \theta_0 + \sigma^2}{\cos^2 \theta_0 - \sigma^2}\right).$$

162 The meridional structure of the gravity modes is determined by the sign of  $((1/4)P^2 - Q)$ . For  
163 given  $m$ , there exists  $\sigma_m^c$  such that

$$\begin{aligned} \mu^2 &\equiv (1/4)P^2 - Q \\ &= \frac{1}{4} \left[ \frac{\sin 2\theta_0}{\cos^2 \theta_0 - \sigma^2} + \cot \theta_0 \right]^2 - \left(\frac{R}{r_e}\right)^2 (\sigma^2 - \cos^2 \theta_0) \\ &\quad + \frac{m^2}{\sin^2 \theta_0} + \frac{m}{\sigma} \left(\frac{\cos^2 \theta_0 + \sigma^2}{\cos^2 \theta_0 - \sigma^2}\right) > 0 \end{aligned}$$

164 when  $1 < \sigma \leq \sigma_m^c$ . When  $\sigma > \sigma_m^c$  the sign of  $\mu^2$  becomes negative. Following the method of  
165 solution in section 3 we obtain the gravity wave dispersion relation in a rotating polar cap:

$$\mu = \left[ \frac{1}{2}P + \frac{m}{\sigma} \cot \theta_B \right] \tanh(\mu \theta_B), \quad (4.2a)$$

166 when  $\mu^2 > 0$  (i.e.  $1 < \sigma \leq \sigma_m^c$ ). When  $\sigma > \sigma_m^c$  the dispersion relation becomes

$$|\mu| = \left[ \frac{1}{2}P + \frac{m}{\sigma} \cot \theta_B \right] \tan(|\mu| \theta_B). \quad (4.2b)$$

167 In the limit when  $\sigma \gg 1$ ,  $P \sim \cot \theta_0$  and  $Q \sim (R/r_e)^2 \sigma^2$  and

$$\mu^2 \sim \left(\frac{1}{4}\right) \cot^2 \theta_0 - \left(\frac{R}{r_e}\right)^2 \sigma^2 \sim -\left(\frac{R}{r_e}\right)^2 \sigma^2.$$

168 The dispersion relation (4.2b) can then be approximated, in this high frequency limit, by

$$X = \frac{1}{2} \cot \theta_B \tan(X \theta_B), \quad (4.3)$$

169 where  $X \equiv \sigma(R/r_e)$ . This high frequency gravity wave limit is, of course, captured by the  
170 “ $f$ -sphere” amplitude equation (2.8). We observe from (4.3) that the gravity wave frequencies

171 become independent of  $m$  in this limit. Table 5 presents the gravity wave mode frequencies  
 172 using the basin parameters listed in Table 1. Table 5 indeed reveals that as  $|m|$  increases the  
 173 eigenfrequencies converge, namely,  $\sigma_{m,n} \sim \sigma_{-m,n}$  as predicted by (4.3). The sensitivity of the  
 174 gravity wave frequencies to  $\theta_0$  is again found to decrease with increasing meridional modal  
 175 number  $n$ . Figure 3 and 4 show the normalised eigenfunctions proportional to the surface  
 176 displacement for low order gravity wave modes,  $\sigma_{m,n}$  has  $n - 1$  nodal circles of amplitude, and  
 177  $m + 1$  distinct cells in the azimuthal direction (i.e.  $m$  nodal diameters). The displacement field  
 178 associated with the modes  $\sigma_{m,1}$  ( $m = \pm 1, \pm 2, \dots$ ) resembles a coastal trapped wave, with amplitude  
 179 monotonically decreasing towards the centre of the basin, although in the contrast with these  
 180 vorticity waves, their propagation is not right-bounded in the Northern Hemisphere.

181  
 182 Interestingly, the asymptotic behaviour of the gravity wave frequencies when  $n$  is large can  
 183 be deduced from the amplitude equation (2.5a) without invoking the IT approximation. First,  
 184 observe that when  $\sigma \gg 1$  (2.5a) can be approximated by

$$F'' + \cot \theta F' + \left( \frac{\sigma R}{r_e} \right)^2 F = 0, \quad (4.4)$$

185 The change of independent variable  $z = \cos \theta$  transforms (4.4) into the ordinary differential equa-  
 186 tion

$$(1 - z^2) F'' - 2z F' + \left( \frac{\sigma R}{r_e} \right)^2 F = 0. \quad (4.5)$$

187 where  $F' \equiv dF/dz$ . Equation (4.5) is the Legendre equation and it is well known that it supports  
 188 bounded solutions on  $[-1, 1]$  only when (see Abramowitz and Stegun 1965, Chapter 22)

$$\left( \frac{\sigma_n R}{r_e} \right)^2 = n(n+1). \quad (4.6)$$

189 In other words, the gravity wave eigenfrequencies become independent of  $m$  when  $\sigma^2 \gg 1$ , and  
 190 (4.6) shows that

$$\sigma_n \sim \frac{r_e}{R} n \quad n \gg 1. \quad (4.7)$$

191 Similar asymptotic behaviour for  $\sigma_n$  follows immediately from (4.3) where  $\sigma_n \sim (r_e/R) (n\pi/\theta_B)$ ,  
 192 where the difference in the constant of proportionality between this expression and (4.7) is due to  
 193 the ‘‘IT approximation’’.

## 194 5. Conclusions and discussions

195 We have derived the governing amplitude equation for azimuthally propagating gravity and  
 196 divergent planetary waves modes in a spherical cap, retaining full spherical geometry. Thereafter,  
 197 we adopt the IT approximation first advanced by Imawaki and Takano (1974), and fixed the  
 198 co-latitude in the coefficients of the governing wave amplitude equation, thereby allowing  
 199 analytical techniques to be used to solve the eigenvalue problem. The planetary wave frequencies  
 200 calculated from the computationally efficient dispersion relation show acceptable agreement with  
 201 their equivalent counterparts in LeBlond (1964) for relatively long azimuthal and meridional  
 202 wavelength eigenfunctions. As these wavelengths decrease the departure between the eigenfre-  
 203 quencies in LeBlond (1964) and in this study, increase. This reflects the fact that short wavelength  
 204 modes are more sensitive to the fixed value of the co-latitude in the IT approximation. We have  
 205 found the gravest mode planetary wave eigenfrequency, which is accurately predicted by the  
 206 dispersion relation derived using the IT approximation, is sensitive to the choice of the co-latitude,  
 207  $\theta_0$ . Values of  $\theta_0$  other than  $0.5\theta_B$  reduce the accuracy of this mode. The sensitivity of  $\sigma_{m,n}$  to  
 208  $\theta_0$  reduces for  $m = -1$  ( $n = 2, \dots, 5$ ), and for these frequencies the IT approximation produces an  
 209 acceptable estimate of their exact value.

210

211 The eigenfrequencies and eigenfunctions (corresponding to the surface displacement) for  
 212 gravity waves modes in a spherical polar cap are also calculated in this study. For a fixed  
 213 azimuthal wavenumber,  $|m|$ , there is a clockwise and counterclockwise propagating gravity wave  
 214 mode, in contrast with the planetary waves. For fixed low values of  $m$  and  $n$  (the meridional  
 215 wavenumber index)  $\sigma_{-m,n} \neq \sigma_{m,n}$ . However, as  $|m|$  increases the frequencies of the clock-  
 216 wise and counterclockwise propagating modes converge in value, as predicted analytically in  
 217 this study. Further, as  $n$  increases,  $\sigma_{m,n}$  increases and the dependence of  $\sigma_{m,n}$  on  $m$  becomes  
 218 weak. Asymptotically, we find that when  $\sigma \gg 1$ ,  $\sigma_{m,n} \propto n$ , with dependence on  $m$  becoming weak.

219  
 220 The high degree of accuracy of the IT approximation in representing steady-state planetary  
 221 flows in a spherical cap has been established by Kitauchi and Ikeda (2009). However, we are  
 222 unaware of any study that addresses how well the IT approximation captures freely propagating  
 223 gravity and vorticity wave dynamics in a spherical cap which is the purpose of this study.  
 224 By fixing  $\theta$  in the wave amplitude equation on a sphere, we are effectively assigning a fixed  
 225 representative value of the meridional gradient of the Coriolis parameter. The resulting free-wave  
 226 dynamics are in qualitative agreement with the planetary waves on a sphere, and for low modes  
 227 there is also good quantitative agreement. For gravity modes at high frequencies (i.e.  $\sigma \gg 1$ ) we  
 228 demonstrate that  $\sigma$  is asymptotically in agreement, as a function of the meridional wavenumber  
 229  $n$ , with the equivalent expression derived using full spherical geometry. We anticipate that the low  
 230 order (long wavelength) planetary wave modes in a layered or a continuously stratified ocean in a  
 231 polar cap will also be accurately represented using the IT approximation.

232 *Acknowledgments.* E.Gavilan gratefully acknowledges the support of a Newcastle University  
 233 research studentship. We thank Miguel Morales Maqueda for his helpful comments on the pre-

234 sentation of the paper. We also thanks two anonymous referees for their helpful and perceptive  
235 comments that have improved the final manuscript.

## 236 **References**

237 Abramowitz, M., and I. A. Stegun, Eds., 1965: *Handbook of Mathematical Functions*. New edition  
238 edition ed., Dover Publications Inc., New York, 1046 pp.

239 Bridger, A. F. C., and D. E. Stevens, 1980: Long Atmospheric Waves and the Polar-Plane Ap-  
240 proximation to the Earths Spherical Geometry. *Journal of the Atmospheric Sciences*, **37** (3),  
241 534–544, doi:10.1175/1520-0469(1980)037<0534:LAWATP>2.0.CO;2.

242 Harlander, U., 2005: A high-latitude quasi-geostrophic delta plane model derived from spherical  
243 geometry. *Tellus A*, **57** (1), 43–54, doi:10.1111/j.1600-0870.2005.00083.x.

244 Haurwitz, B., 1975: Long circumpolar atmospheric waves. *Archiv fr Meteorologie, Geophysik und*  
245 *Bioklimatologie, Serie A*, **24** (1), 1–18, doi:10.1007/BF02247554.

246 Imawaki, S., and K. Takano, 1974: Planetary flow in a circular basin. *Deep Sea Research and*  
247 *Oceanographic Abstracts*, **21** (1), 69–IN3, doi:10.1016/0011-7471(74)90020-5.

248 Kitauchi, H., and M. Ikeda, 2009: An analytic solution of steady Stokes flow on a rotating polar  
249 cap. *Fluid Dynamics Research*, **41** (4), 045 505, doi:10.1088/0169-5983/41/4/045505.

250 LeBlond, P. H., 1964: Planetary waves in a symmetrical polar basin. *Tellus*, **16** (4), 503–512,  
251 doi:10.1111/j.2153-3490.1964.tb00185.x.

252 Longuet-Higgins, M. S., 1968: The Eigenfunctions of Laplace’s Tidal Equations over a Sphere.  
253 *Philosophical Transactions of the Royal Society of London A: Mathematical, Physical and En-*  
254 *gineering Sciences*, **262** (1132), 511–607, doi:10.1098/rsta.1968.0003.



- 255 Paldor, N., 2015: *Shallow Water Waves on the Rotating Earth*. SpringerBriefs in Earth System  
256 Sciences ed., Springer International Publishing, 77 pp.
- 257 Paldor, N., Y. De-Leon, and O. Shamir, 2013: Planetary (Rossby) waves and inertia–gravity  
258 (Poincaré) waves in a barotropic ocean over a sphere. *Journal of Fluid Mechanics*, **726**, 123–  
259 136, doi:10.1017/jfm.2013.219.

260	<b>LIST OF TABLES</b>	
261	<b>Table 1.</b>	Parameter values used by LeBlond (1964) and also employed in this study . . . . 18
262	<b>Table 2.</b>	Eigenfrequencies $\sigma_{m,n}$ determined from the full dispersion relation (3.3) . . . . 19
263	<b>Table 3.</b>	Percentage error of the wave frequencies calculated using the dispersion rela-
264		tion (3.3) and the polar-plane approximation in LeBlond (1964). . . . . 20
265	<b>Table 4.</b>	Sensitivity of the planetary wave eigenfrequencies to the choice of the co-
266		latitude $\theta_0$ , as measured by $ \sigma(0.75\theta_B) - \sigma(0.5\theta_B) /\sigma(0.5\theta_B)$ , expressed as
267		a percentage. . . . . 21
268	<b>Table 5.</b>	Gravity wave frequencies calculated from (4.2) using the basin parameters in
269		Table 1 . . . . . 22

Symbol	Variable(Unit)	Value
$\Omega$	Angular velocity of the Earth ( $s^{-1}$ )	$7.292 \times 10^{-5}$
$R$	Radius of the Earth ( $m$ )	$6.370 \times 10^6$
$g$	Gravitational acceleration ( $ms^{-2}$ )	9.8
$H$	Depth of the basin ( $m$ )	5753
$\theta_B$	Co-latitude at the boundary ( <i>degrees</i> )	12.92

TABLE 1. Parameter values used by LeBlond (1964) and also employed in this study

---

$m =$	$-1$	$-2$	$-3$	$-4$
-------	------	------	------	------

---

$n = 1$	0.00325	0.00367	0.00319	0.00268
2	0.00112	0.00178	0.00197	0.00193
3	0.00054	0.00095	0.00120	0.00131
4	0.00031	0.00058	0.00078	0.00091
5	0.00020	0.00038	0.00054	0.00065

---

TABLE 2. Eigenfrequencies  $\sigma_{m,n}$  determined from the full dispersion relation (3.3)

---

$m =$	$-1$	$-2$	$-3$	$-4$
-------	------	------	------	------

---

$n = 1$	0.40	0.45	13.39	27.99
2	11.03	21.34	20.77	15.77
3	10.82	22.79	26.78	26.57
4	9.75	21.36	27.07	29.23
5	8.76	19.56	25.87	29.24

---

270      TABLE 3. Percentage error of the wave frequencies calculated using the dispersion relation (3.3) and the  
271      polar-plane approximation in LeBlond (1964).

---

$m =$	$-1$	$-2$	$-3$	$-4$
-------	------	------	------	------

---

$n = 1$	21.85	51.95	75.58	90.77
2	6.59	19.8	36.24	52.09
3	3.04	9.74	19.39	30.44
4	1.73	5.69	11.74	19.25
5	1.12	3.71	7.79	13.06

---

TABLE 4. Sensitivity of the planetary wave eigenfrequencies to the choice of the co-latitude  $\theta_0$ , as measured by  $|\sigma(0.75\theta_B) - \sigma(0.5\theta_B)|/\sigma(0.5\theta_B)$ , expressed as a percentage.

---

$m =$	-4	-3	-2	-1	1	2	3	4
-------	----	----	----	----	---	---	---	---

---

$n = 1$	9.2928	7.0865	4.9357	2.9444	2.3844	4.5927	6.8469	9.1101
2	10.571	8.6917	7.0417	5.815	5.7373	6.9357	8.5877	10.478
3	12.74	11.228	10.004	9.1854	9.1546	9.9523	11.166	12.676
4	15.435	14.212	13.268	12.663	12.647	13.238	14.173	15.391
5	18.427	17.416	16.654	16.178	16.168	16.636	17.39	18.396

---

TABLE 5. Gravity wave frequencies calculated from (4.2) using the basin parameters in Table 1

274	<b>LIST OF FIGURES</b>	
275	<b>Fig. 1.</b> Schematic of the spherical polar coordinate system showing the unit vectors $\mathbf{k}$ , $\hat{\theta}$ and $\hat{\varphi}$ that	
276	form a right-handed triad . . . . .	24
277	<b>Fig. 2.</b> Plot of the planetary waves frequencies $\sigma_{-1,n}$ ( $n = 1, \dots, 5$ ) as a function of $\varepsilon^2 = (r_e/R)^2$	
278	when $\theta_0 = 0.5\theta_B$ . . . . .	25
279	<b>Fig. 3.</b> Eigenfunctions associated with gravity wave modes. The dashed (solid) line represent neg-	
280	ative (positive) values of sea surface elevation. a) $\sigma_{-1,1}$ ; b) $\sigma_{1,1}$ ; c) $\sigma_{-1,2}$ ; d) $\sigma_{1,2}$ . The	
281	patterns rotate counterclockwise (clockwise) for $m \geq 1$ ( $m \leq -1$ ). . . . .	26
282	<b>Fig. 4.</b> As in figure 2 except for a) $\sigma_{-2,1}$ ; b) $\sigma_{2,1}$ ; c) $\sigma_{-2,2}$ ; d) $\sigma_{2,2}$ . . . . .	27



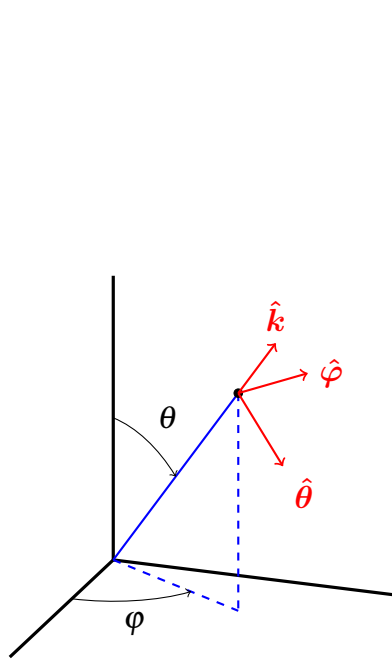


FIG. 1. Schematic of the spherical polar coordinate system showing the unit vectors  $\hat{k}$ ,  $\hat{\theta}$  and  $\hat{\varphi}$  that form a right-handed triad

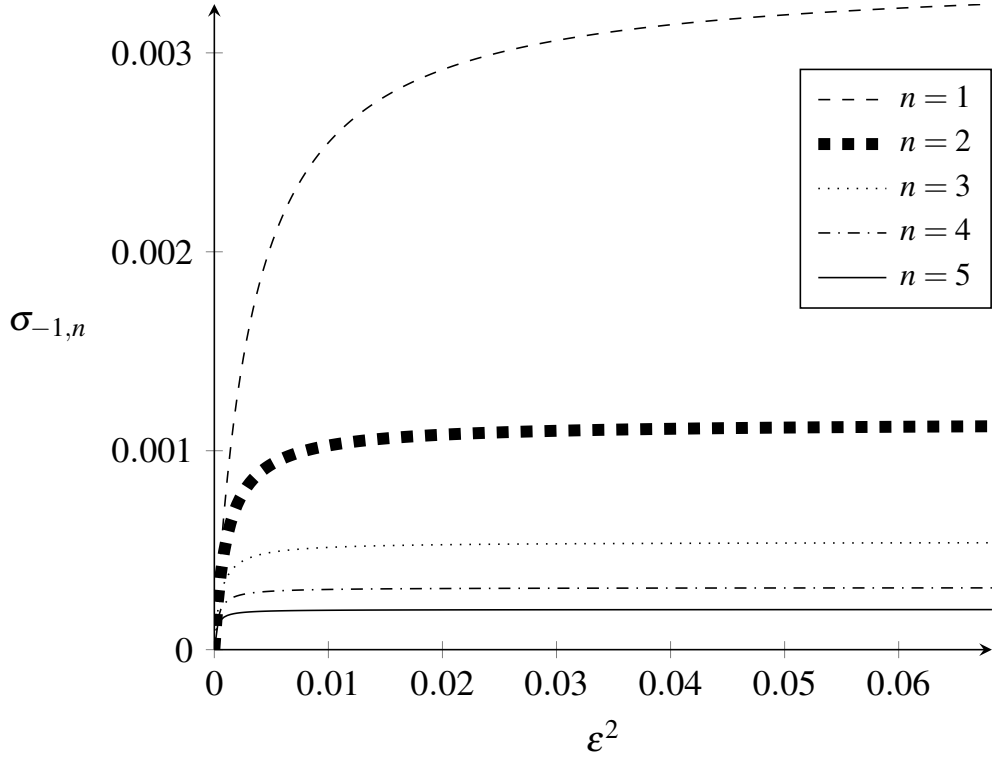
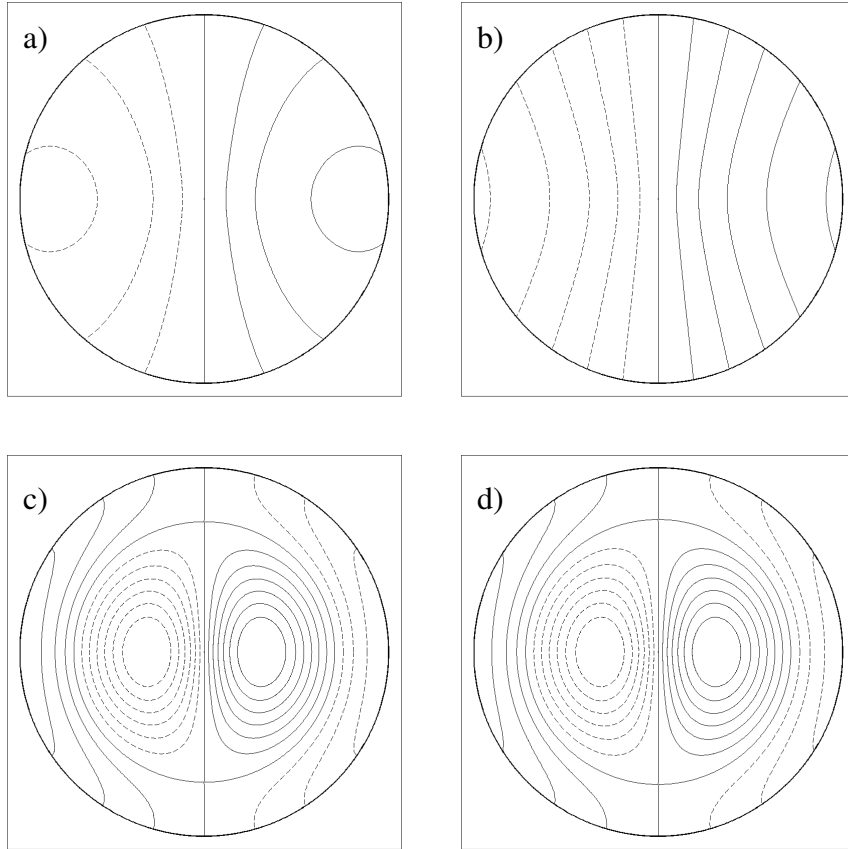


FIG. 2. Plot of the planetary waves frequencies  $\sigma_{-1,n}$  ( $n = 1, \dots, 5$ ) as a function of  $\varepsilon^2 = (r_e/R)^2$  when  $\theta_0 = 0.5\theta_B$ .



285 FIG. 3. Eigenfunctions associated with gravity wave modes. The dashed (solid) line represent negative  
 286 (positive) values of sea surface elevation. a)  $\sigma_{-1,1}$ ; b)  $\sigma_{1,1}$ ; c)  $\sigma_{-1,2}$ ; d)  $\sigma_{1,2}$ . The patterns rotate counterclockwise  
 287 (clockwise) for  $m \geq 1$  ( $m \leq -1$ ).

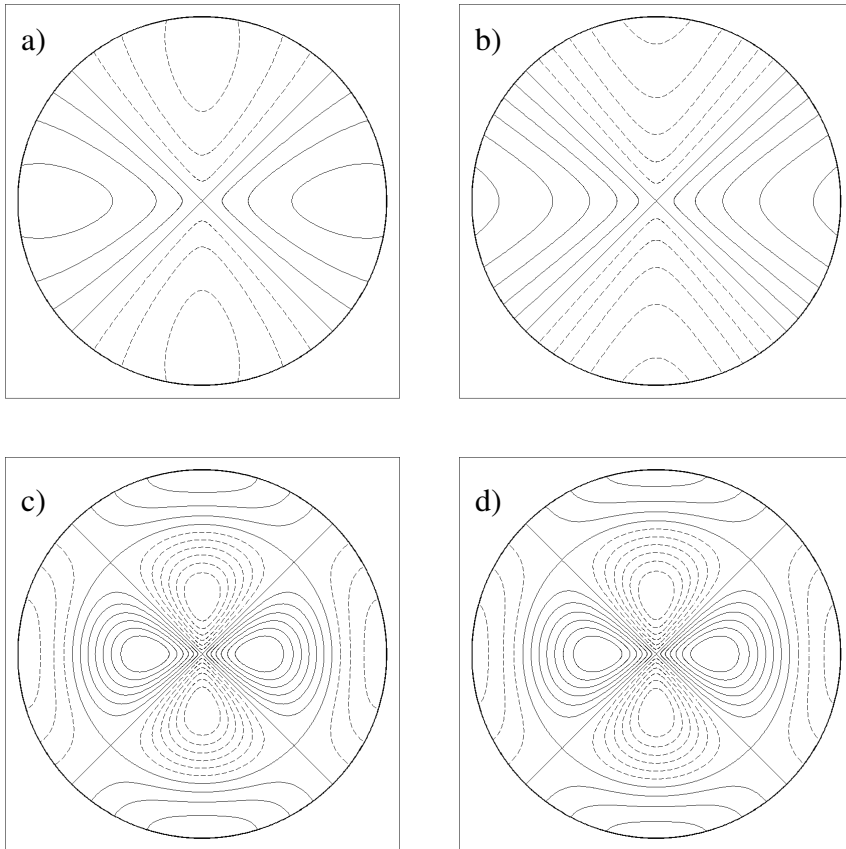


FIG. 4. As in figure 2 except for a)  $\sigma_{-2,1}$ ; b)  $\sigma_{2,1}$ ; c)  $\sigma_{-2,2}$ ; d)  $\sigma_{2,2}$ .